Inorg. Chem. **2008**, *47*, 3384−3392

Arylthiolate Coordination and Reactivity at Pseudotetrahedral Nickel(II) Centers: Modulation by Noncovalent Interactions

Swarup Chattopadhyay,[†] Tapash Deb,[†] Huaibo Ma,[†] Jeffrey L. Petersen,[‡] Victor G. Young, Jr.,[§] and Michael P. Jensen*[,†]

Department of Chemistry and Biochemistry, Ohio University, Athens, Ohio 45701, C. Eugene Bennett Department of Chemistry, West Virginia University, Morgantown, West Virginia 26506, and X-ray Crystallographic Laboratory, Department of Chemistry, University of Minnesota, Minneapolis, Minnesota 55455

Received December 13, 2007

Five new pseudotetrahedral nickel(II) arylthiolate complexes $Tp^{R,Me}Ni-SR'$ [$(Tp^{R,Me})^- = 2,2,2\text{-}\kappa^3$-hydridotris(3-R,5-methylpyrazolyl)borate; R = Me, R′ = C_6H_5 (Ph), 2,4,6-$C_6H_2(CH_3)_3$ (Mes); R = Ph, R′ = C_6H_5 (Ph), 2,4,6-$C_6H_2(CH_3)_3$ (Mes), and 2,6-$C_6H_3(CH_3)_2$ (Xyl)] were prepared by metathesis reactions of known chloride complexes with sodium arylthiolate salts in THF. The new products were fully characterized. The effect of increasing bulk of substituents at the proximal 3-pyrazolyl and ortho-thiolate positions represented in this series was evident in spectroscopic studies (UV–vis-NIR, ^{1}H NMR) of the product complexes. Increased steric contact induced red-shifting of nickel-thiolate ligand to metal charge transfer (LMCT) bands and enhanced contact shifts of arylthiolate protons with the paramagnetic ($S = 1$) nickel(II) ion. These spectroscopic effects arise from structural distortion of the nickel(II)-thiolate bond revealed by X-ray crystal structure determinations of the structural extremes of the series, $Tp^{Me,Me}Ni-SPh$ and $Tp^{Ph,Me}Ni-SXyl$. The distortion consists of a significantly increased tilting of the Ni−S bond from an ideal trigonal axis and increased linearity of the Ni−S−R angle that alters covalency of the Ni−S coordinate bond. Reactivity of the nickel-thiolate linkage toward electrophilic alkylation with MeI is also significantly affected, showing enhanced rates according to two distinct competing mechanisms, direct bimolecular alkylation of intact complex and rate-limiting unimolecular dissociation of free thiolate. Possible biochemical relevance of these observations to tetrahedral nickel(II) centers in metalloenzymes is considered.

1. Introduction

The ongoing renaissance in structural biology has recently yielded X-ray crystallographic structures of several metalloenzymes that certain anaerobic bacteria and archaebacteria utilize to support metabolic bio-organometallic reactivity, in which carbon dioxide, methane, and acetate are interconverted on a gigaton per year scale, significantly impacting the global carbon cycle.[1–3] The active sites of these enzymes, including the A- and C-clusters of acetyl coenzyme-A synthase/carbon monoxide dehydrogenase (ACS/CODH) and acetyl coenzyme-A decarbonylase/synthase (ACDS),[4–9] bimetallic Fe/Ni sites in hydrogenases,[10,11] and the F430 cofactor of methyl-coenzyme M reductase (MCR),[12] all

* To whom correspondence should be addressed. E-mail: jensenm@ohio.edu.
† Ohio University.
‡ West Virginia University.
§ University of Minnesota.

(1) Ragsdale, S. W. *J. Inorg. Biochem.* **2007**, *101*, 1657–1666.
(2) Drennan, C. L.; Doukov, T. I.; Ragsdale, S. W. *J. Biol. Inorg. Chem.* **2004**, *9*, 511–515.
(3) Ermler, U. *Dalton Trans.* **2005**, 3451–3458.
(4) Drennan, C. L.; Heo, J.; Sintchak, M. D.; Schreiter, E.; Ludden, P. W. *Proc. Natl. Acad. Sci. USA* **2001**, *98*, 11973–11978.
(5) Dobbek, H.; Svetlitchnyi, V.; Gremer, L; Huber, R.; Meyer, O. *Science* **2001**, *293*, 1281–1285.
(6) Doukov, T. I.; Iverson, T. M.; Seravalli, J.; Ragsdale, S. W.; Drennan, C. L. *Science* **2002**, *298*, 567–572.
(7) Darnault, C.; Volbeda, A.; Kim, E. J.; Legrand, P.; Vernède, X.; Lindahl, P. A.; Fontecilla-Camps, J. C. *Nat. Struct. Biol.* **2003**, *10*, 271–279.
(8) Svetlitchnyi, V.; Dobbek, H.; Meyer-Klaucke, W.; Meins, T.; Thiele, B.; Römer, P.; Huber, R.; Meyer, O. *Proc. Natl. Acad. Sci. USA* **2004**, *101*, 446–451.
(9) Jeoung, J.-H.; Dobbek, H. *Science* **2007**, *318*, 1461–1464.
(10) Volbeda, A.; Charon, M.-H.; Piras, C.; Hatchikian, E. C.; Frey, M.; Fontecilla-Camps, J. C. *Nature* **1995**, *373*, 580–587.
(11) Fontecilla-Camps, J. C.; Volbeda, A.; Cavazza, C.; Nicolet, Y. *Chem. Rev.* **2007**, *107*, 4273–4303.
(12) Ermler, U.; Grabarse, W.; Shima, S.; Goubeaud, M.; Thauer, R. K. *Science* **1997**, *278*, 1457–1462.

10.1021/ic702417w CCC: $40.75
Published on Web 03/15/2008

feature essential nickel ions.[13–19] Moreover, the metal-centered enzymatic activities have strong evolutionary links to organosulfur chemistry, either as active-site ligation to nickel, or in essential cofactors.[20,21] Sulfur-ligated nickel ions were recently found in a superoxide dismutase[22,23] and in nickel-dependent transcription factors.[24,25] Nickel(II) ions have also been introduced into cysteine-ligated binding sites as spectroscopic and structural probes in rubredoxin,[26,27] azurin,[28,29] the aspartate transcarbamoylase regulatory domain,[30] and zinc fingers.[31]

The ACS A-cluster turnover plausibly occurs through a formally diamagnetic Ni(0)/Ni(II) couple at the proximal nickel,[7,32,35] and several elegant ACS model reactions using synthetic diamagnetic complexes have been reported.[36–42] On the other hand, in many of the cases just cited, the resting active-site nickel is supported within a weak ligand field in a divalent, high-spin state (d^8, $S = 1$). Examples include reduced hydrogenase[43,44] and the ACDS A-cluster proximal nickel;[17,18] the ACS A-cluster proximal site can also adopt a tetrahedral geometry about divalent metal ions.[7] Comparatively less is known about relevant organometallic and organosulfur coordination chemistry of tetrahedral high-spin nickel(II).

Considering the relevant example of small-molecule complexes of experimentally convenient arylthiolates, the Cambridge Structural Database presently returns only 59 examples of discrete terminal complexes, of which 42 are diamagnetic. Several paramagnetic complexes are found with linear,[45] square-pyramidal,[46–48] trigonal-bipyramidal,[49–52] and octahedral geometries;[49,53] pseudotetrahedral examples include only five complex ions of general formula $[Ni(SAr)_4]^{2-}$,[54–57] plus five recently reported complexes of general formula (κ^3-L)NiSAr, where L is a tripodal anionic borate with appended organophosphine,[58] pyrazolyl,[59] or organosulfide[60] donors. Further elucidation of biomimetic organosulfur chemistry at paramagnetic nickel(II) centers thus retains significant impetus.

We describe in the present work additional examples of pseudotetrahedral arylthiolate complexes of nickel(II) supported by tris(pyrazolyl)borate ligands. Moreover, we have adopted a distinctive approach by focusing exclusively on complexes in which proximal substituents on the 3-pyrazolyl and ortho-arylthiolate carbons are varied to manipulate thiolate coordination through noncovalent steric contact (Scheme 1). In particular, the tris(pyrazolyl)borate complexes $Tp^{R,Me}Ni-SR'$ [R = Me (**1**), Ph (**2**); R′ = C_6H_5, Ph (**a**); 2,4,6-$C_6H_2Me_3$, Mes (**b**); 2,6-$C_6H_3Me_2$, Xyl (**c**)] were prepared and characterized. The resulting series of sterically modified complexes **1a,b** and **2a**−**c** reveals significant and unprec-

(13) Bramlett, M. R.; Tan, X.; Lindahl, P. A. *J. Am. Chem. Soc.* **2003**, *125*, 9316–9317.
(14) Tan, X.; Bramlett, M. R.; Lindahl, P. A. *J. Am. Chem. Soc.* **2004**, *126*, 5954–5955.
(15) Seravalli, J.; Xiao, Y.; Gu, W.; Cramer, S. P.; Antholine, W. E.; Krymov, V.; Gerfen, G. J.; Ragsdale, S. W. *Biochemistry* **2004**, *43*, 3944–3955.
(16) Gencic, S; Grahame, D. A. *J. Biol. Chem.* **2003**, *278*, 6101–6110.
(17) Gu, W.; Gencic, S.; Cramer, S. P.; Grahame, D. A. *J. Am. Chem. Soc.* **2003**, *125*, 15343–15351.
(18) Funk, T.; Gu, W.; Friedrich, S.; Wang, H.; Gencic, S.; Grahame, D. A.; Cramer, S. P. *J. Am. Chem. Soc.* **2004**, *126*, 88–95.
(19) Dey, M.; Telser, J.; Kunz, R. C.; Lees, N. S.; Ragsdale, S. W.; Hoffman, B. M. *J. Am. Chem. Soc.* **2007**, *129*, 11030–11032.
(20) Huber, C.; Wächtershäuser, G. *Science* **1997**, *276*, 245–247.
(21) Russell, M. J.; Martin, W. *Trends. Biochem. Sci.* **2004**, *29*, 358–363.
(22) Barondeau, D. P.; Kassman, C. J.; Bruns, C. K.; Tainer, J. A.; Getzoff, E. D. *Biochemistry* **2004**, *43*, 8038–8047.
(23) Wuerges, J.; Lee, J.-W.; Yim, Y.-I.; Yim, H.-S.; Kang, S.-O.; Djinovic Carugo, K. *Proc. Natl. Acad. Sci. USA* **2004**, *101*, 8569–8574.
(24) Schreiter, E. R.; Sintchak, M. D.; Guo, Y.; Chivers, P. T.; Sauer, R. T.; Drennan, C. L. *Nat. Struct. Biol.* **2003**, *10*, 794–799.
(25) Dian, C.; Schauer, K.; Kapp, U.; McSweeney, S. M.; Labigne, A.; Terradot, L. *J. Mol. Biol.* **2006**, *361*, 715–730.
(26) Kowal, A. T.; Zambrano, I. C.; Moura, I.; Moura, J. J. G.; LeGall, J.; Johnson, M. K. *Inorg. Chem.* **1988**, *27*, 1162–1166.
(27) Huang, Y.-H.; Moura, I.; Moura, J. J. G.; LeGall, J.; Park, J.-B.; Adams, M. W. W.; Johnson, M. K. *Inorg. Chem.* **1993**, *32*, 406–412.
(28) Tennent, D. L.; McMillin, D. R. *J. Am. Chem. Soc.* **1979**, *101*, 2307–2311.
(29) Hannan, J. P.; Davy, S. L.; Moore, G. R.; Eady, R. R.; Andrew, C. R. *J. Biol. Inorg. Chem.* **1998**, *3*, 282–291.
(30) Johnson, R. S.; Schachman, H. K. *Proc. Natl. Acad. Sci. USA* **1980**, *77*, 1995–1999.
(31) Krizek, B. A.; Berg, J. M. *Inorg. Chem.* **1992**, *31*, 2984–2986.
(32) Lindahl, P. A. *J. Biol. Inorg. Chem.* **2004**, *9*, 516–524.
(33) Webster, C. E.; Darensbourg, M. Y.; Lindahl, P. A.; Hall, M. B. *J. Am. Chem. Soc.* **2004**, *126*, 3410–3411.
(34) Tan, X.; Surovtsev, I. V.; Lindahl, P. A. *J. Am. Chem. Soc.* **2006**, *128*, 12331–12338.
(35) Bramlett, M. R.; Stubna, A.; Tan, X.; Surovtsev, I. V.; Münck, E.; Lindahl, P. A. *Biochemistry* **2006**, *45*, 8674–8685.
(36) Stavropoulos, P.; Carrié, M.; Muetterties, M. C.; Holm, R. H. *J. Am. Chem. Soc.* **1990**, *112*, 5385–5387.
(37) Stavropoulos, P.; Muetterties, M. C.; Carrié, M.; Holm, R. H. *J. Am. Chem. Soc.* **1991**, *113*, 8485–8492.
(38) Hsiao, Y.-M.; Chojnacki, S. S.; Hinton, P.; Reibenspies, J. H.; Darensbourg, M. Y. *Organometallics* **1993**, *12*, 870–875.
(39) Matsunaga, P. T.; Hillhouse, G. L. *Angew. Chem. Int. Ed* **1994**, *33*, 1748–1749.
(40) Tucci, G. C.; Holm, R. H. *J. Am. Chem. Soc.* **1995**, *117*, 6489–6496.
(41) Sellmann, D.; Häussinger, D.; Knoch, F.; Moll, M. *J. Am. Chem. Soc.* **1996**, *118*, 5368–5374.
(42) Eckert, N. A.; Dougherty, W. G.; Yap, G. P. A.; Riordan, C. G. *J. Am. Chem. Soc.* **2007**, *129*, 9286–9287.
(43) Wang, H.; Ralston, C. Y.; Patil, D. S.; Jones, R. M.; Gu, W.; Verhagen, M.; Adams, M.; Ge, P.; Riordan, C.; Marganian, C. A.; Mascharak, P.; Kovacs, J.; Miller, C. G.; Collins, T. J.; Brooker, S.; Croucher, P. D.; Wang, K.; Stiefel, E. I.; Cramer, S. P. *J. Am. Chem. Soc.* **2000**, *122*, 10544–10552.
(44) Fan, H.-J.; Hall, M. B. *J. Am. Chem. Soc.* **2002**, *124*, 394–395.
(45) Nguyen, T.; Panda, A.; Olmstead, M. M.; Richards, A. F.; Stender, M.; Brynda, M.; Power, P. P. *J. Am. Chem. Soc.* **2005**, *127*, 8545–8552.
(46) Ram, M. S.; Riordan, C. G.; Ostrander, R.; Rheingold, A. L. *Inorg. Chem.* **1995**, *34*, 5884–5892.
(47) Wilker, J. J.; Gelasco, A.; Pressler, M. A.; Day, R. O.; Maroney, M. J. *J. Am. Chem. Soc.* **1991**, *113*, 6342–6343.
(48) Fox, D. C.; Fiedler, A. T.; Halfen, H. L.; Brunold, T. C.; Halfen, J. A. *J. Am. Chem. Soc.* **2004**, *126*, 7627–7638.
(49) Baidya, N.; Olmstead, M.; Mascharak, P. K. *Inorg. Chem.* **1991**, *30*, 929–937.
(50) Baidya, N.; Olmstead, M. M.; Whitehead, J. P.; Bagyinka, C.; Maroney, M. J.; Mascharak, P. K. *Inorg. Chem.* **1992**, *31*, 3612–3619.
(51) Baidya, N.; Olmstead, M. M.; Mascharak, P. K. *J. Am. Chem. Soc.* **1992**, *114*, 9666–9668.
(52) Marganian, C. A.; Vazir, H.; Baidya, N.; Olmstead, M. M.; Mascharak, P. K. *J. Am. Chem. Soc.* **1995**, *117*, 1584–1594.
(53) Osakada, K.; Yamamoto, T.; Yamamoto, A.; Takenaka, A.; Sasada, Y. *Acta. Cryst. C* **1984**, *40*, 85–87.
(54) Swenson, D.; Baenziger, N. C.; Coucouvanis, D. *J. Am. Chem. Soc.* **1978**, *100*, 1932–1934.
(55) Rosenfield, S. G.; Armstrong, W. H.; Mascharak, P. K. *Inorg. Chem.* **1986**, *25*, 3014–3018.
(56) Silver, A.; Koch, S. A.; Millar, M. *Inorg. Chim. Acta* **1993**, *205*, 9–14.
(57) Mueller, A.; Henkel, G. *Z. Naturforsch. B* **1995**, *50*, 1464–1468.
(58) MacBeth, C. E.; Thomas, J. C.; Betley, T. A.; Peters, J. C. *Inorg. Chem.* **2004**, *43*, 4645–4662.
(59) Matsunaga, Y.; Fujisawa, K.; Ibi, N.; Miyashita, Y.; Okamoto, K.-i *Inorg. Chem.* **2005**, *44*, 325–335.
(60) Cho, J.; Yap, G. P. A.; Riordan, C. G. *Inorg. Chem.* **2007**, *46*, 11308–11315.

Scheme 1

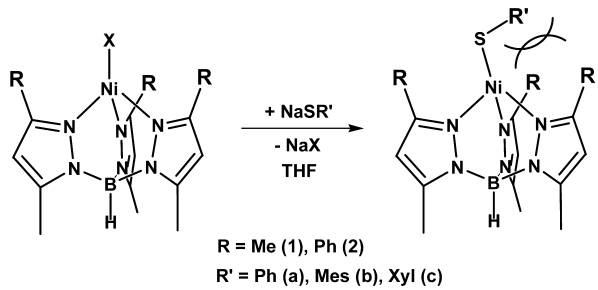

edented correlations between spectroscopy, structure, and reactivity that further illuminate metal−sulfur coordinate bonding at tetrahedral nickel(II).

2. Experimental Details

General Procedures. All materials obtained from commercial vendors were ACS reagent-grade or better and were used as received, except for drying of solvents by routine techniques. All manipulations were carried out under an inert atmosphere of prepurified argon, either in a glovebox (MBraun Unilab) or using Schlenk techniques. Known $Tp^{R,Me}NiCl$ complexes (R = Me, Ph) were prepared by modification of literature procedures,[61–63] from metatheses of anhydrous $NiCl_2$ and $TlTp^{R,Me}$ in $MeOH/CH_2Cl_2$ (**Caution!** *Thallium salts are extremely toxic and must be properly handled and disposed of*). Aromatic thiols were purchased from Aldrich and converted to sodium salts by titration of $NaNH_2$ in toluene. ^1H NMR data were recorded on a Varian Unity 500 spectrometer and processed using the MestReNova software suite (Mestrelab Research, Santiago de Compostela, Spain); spectra were referenced internally to residual $CHCl_3$ solvent (7.24 ppm), and experimental temperatures were calibrated by the methanol method using Varian software. Solution magnetic moments of **1a** and **2b** were determined by the Evans NMR method in $CDCl_3$ at 295 K.[64] FT-IR spectra were recorded from KBr pellets on a Thermo-Electron Nicolet 380 spectrophotometer. UV–visible-NIR spectra were recorded on an Agilent HP-8453 diode-array spectrophotometer; kinetic data were analyzed using the SPECFIT software package (Spectrum Software Associates, Marlborough, MA). Elemental analyses were performed by Atlantic Microlabs, Inc. (Norcross, GA).

Preparation of $Tp^{Me,Me}Ni-SPh$ (1a). To the solution of $Tp^{Me,Me}NiCl$ (75 mg, 0.19 mmol) in THF (20 mL) was added dropwise a solution of NaSPh (38 mg, 0.29 mmol) in THF (15 mL). The color of the solution changed from pale pink to intense red. The mixture was stirred 2 h, and then, solvent was removed under vacuum. The resulting red solid was extracted into toluene (20 mL). The extracts were filtered and evaporated to yield a red powder. Yield: 68 mg (76%). Anal. Calc'd. (found) for $C_{21}H_{27}BN_6NiS$: C, 54.23 (54.64); H, 5.85 (5.98); N 18.07 (18.24). ν (B−H): 2520 cm^{-1}. ^1H NMR ($CDCl_3$; δ, ppm): 77.2 (3H, 4-pz); 23.3 (2H, meta); 6.6 (9H, 5-Me); −7.1 (9H, 3-Me); −10.7 (1H, B-*H*); −18.9 (2H, ortho); −26.6 (1H, para). μ_{eff} = 2.92 μ_B. UV–vis (CH_2Cl_2, λ_{max}, nm; ε, mM^{-1} cm^{-1}): 354 (1.6); 464 (2.4); 506 (2.6); 614 (sh, 0.2); 836 (0.2).

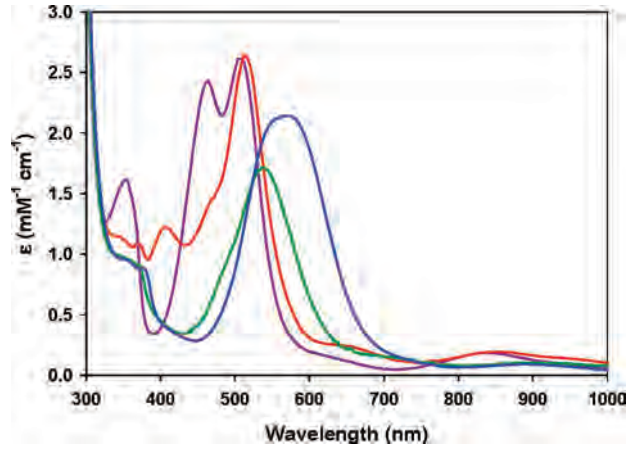

Figure 1. UV–vis-NIR spectra at 297 K in CH_2Cl_2 solution for the following: $Tp^{Me,Me}Ni-SPh$ (**1a**, magenta trace); $Tp^{Me,Me}Ni-SMes$ (**1b**, red); $Tp^{Ph,Me}Ni-SPh$ (**2a**, green); and $Tp^{Ph,Me}Ni-SMes$ (**2b**, blue).

Preparation of $Tp^{Me,Me}Ni-SMes$ (1b). The red complex was prepared as for **1a** above. Yield: 71 mg (73%). Anal. Calcd. (found) for $C_{24}H_{33}BN_6NiS$: C, 56.84 (56.75); H, 6.56 (6.59); N 16.57 (17.32). ν (B−H): 2518 cm^{-1}. ^1H NMR ($CDCl_3$; δ, ppm): 75.0 (3H, 4-pz); 33.3 (6H, ortho); 25.8 (3H, para); 25.3 (2H, meta); 5.2 (9H, 5-Me); −7.5 (9H, 3-Me); −11.3 (1H, B-*H*). UV–vis (CH_2Cl_2, λ_{max}, nm; ε, mM^{-1} cm^{-1}): 343 (1.1); 371 (1.1); 406 (1.2); 467 (sh, 1.5); 514 (2.7); 636 (0.3); 861 (0.2).

Preparation of $Tp^{Ph,Me}Ni-SPh$ (2a). The purple complex was prepared as for **1a** above. Yield: 59 mg (70%). Anal. Calcd. (found) for $C_{36}H_{33}BN_6NiS$: C, 66.39 (67.44); H, 5.11 (5.63); N 12.90 (13.03). ν (B−H): 2548 cm^{-1}. ^1H NMR ($CDCl_3$; δ, ppm): 70.8 (3H, 4-pz); 25.5 (2H, meta); 10.5 (6H, 3-*o*-Ph); 7.8 (6H, 3-*m*-Ph); 7.4 (3H, 3-*p*-Ph); 4.6 (9H, 5-Me); −10.6 (1H, B-*H*); −27.8 (2H, ortho); −37.6 (1H, para). UV–vis (CH_2Cl_2, λ_{max}, nm; ε, mM^{-1} cm^{-1}): 372 (0.9); 489 (sh, 1.0); 537 (1.7); 700 (0.2); 905 (0.2).

Preparation of $Tp^{Ph,Me}Ni-SMes$ (2b). The blue complex was prepared as for **1a** above. Yield: 70 mg (78%). Anal. Calcd. (found) for $C_{39}H_{39}BN_6NiS$: C, 67.57 (67.30); H, 5.67 (5.82); N 12.12 (11.89). ν (B−H): 2540 cm^{-1}. ^1H NMR ($CDCl_3$; δ, ppm): 91.8 (6H, ortho); 67.0 (3H, 4-pz); 57.2 (3H, para); 32.2 (2H, meta); 9.9 (6H, 3-*o*-Ph); 7.4 (6H, 3-*m*-Ph); 7.2 (3H, 3-*p*-Ph); 2.5 (9H, 5-Me); −11.2 (1H, B-*H*). μ_{eff} = 2.83 μ_B. UV–vis (CH_2Cl_2, λ_{max}, nm; ε, mM^{-1} cm^{-1}): 352 (1.0); 378 (0.9); 551 (sh, 2.1); 574 (2.2); 884 (0.1).

Preparation of $Tp^{Ph,Me}Ni-SXyl$ (2c). The purple complex was prepared as for **1a** above. Yield: 66 mg (75%). Anal. Calcd. (found) for $C_{38}H_{37}BN_6NiS$: C, 67.19 (67.14); H, 5.49 (5.48); N 12.37 (12.51). ν (B−H): 2543 cm^{-1}. ^1H NMR ($CDCl_3$; δ, ppm): 97.1 (6H, ortho); 68.0 (3H, 4-pz); 32.9 (2H, meta); 9.9 (6H, 3-*o*-Ph); 7.4 (6H, 3-*m*-Ph); 7.2 (3H, 3-*p*-Ph); 2.5 (9H, 5-Me); −11.4 (1H, B-*H*); −43.2 (1H, para). UV–vis (CH_2Cl_2, λ_{max}, nm; ε, mM^{-1} cm^{-1}): 353 (1.3); 373 (1.3); 543 (2.2); 574 (sh, 2.0); 700 (sh, 0.2); 893 (0.2).

X-ray Crystallography. Diffraction-quality crystals of **1a** and **2c**·$2CH_3CN$ were grown from acetonitrile solutions at −37 °C. Data collections and refinement parameters are summarized in Table 2. Bond lengths and angles are summarized in Table 3. ORTEP diagrams of the complexes are illustrated in Figure 4.

Experimental work on **1a** was conducted at West Virginia University (JLP). A reddish-orange crystal (0.10 × 0.21 × 0.58 mm^3) was washed with perfluoroether PFO-XR75 (Lancaster) and sealed under N_2 in a glass capillary. The sample was optically

(61) Desrochers, P. J.; Cutts, R. W.; Rice, P. K.; Golden, M. L.; Graham, J. B.; Barclay, T. M.; Cordes, A. W. *Inorg. Chem.* **1999**, *38*, 5690–5694.
(62) Uehara, K.; Hikichi, S.; Akita, M. *J. Chem. Soc., Dalton Trans.* **2002**, 3529–3538.
(63) Desrochers, P. J.; LeLievre, S.; Johnson, R. J.; Lamb, B. T.; Phelps, A. L.; Cordes, A. W.; Gu, W.; Cramer, S. P. *Inorg. Chem.* **2003**, *42*, 7945–7950.
(64) Evans, D. F.; Jakubovic, D. A. *J. Chem. Soc., Dalton Trans.* **1988**, 2927–2933.

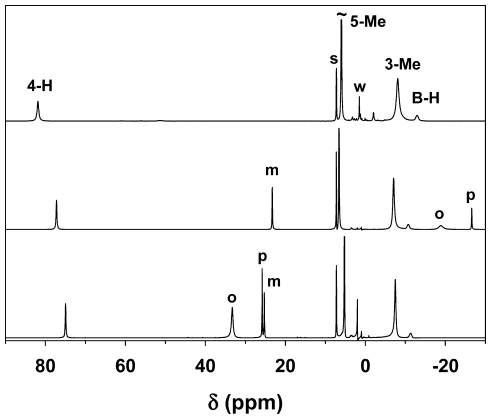

Figure 2. ^{1}H NMR spectra recorded at 293 K in $CDCl_3$ solution for the following: $Tp^{Me,Me}Ni-Cl$, top (labels indicate tris(pyrazolylborate) resonances, *s* = residual solvent, *w* = water); $Tp^{Me,Me}Ni-SPh$, middle (labels indicate arylthiolate resonances); and $Tp^{Me,Me}Ni-SMes$, bottom.

aligned on the four-circle of a Siemens P4 diffractometer equipped with a graphite monochromator, a monocap collimator, a Mo Ka radiation source ($\lambda = 0.71073$ Å), and a SMART CCD detector. The program SMART (version 5.6)[65] was used for diffractometer control, frame scans, indexing, orientation matrix calculations, least-squares refinement of cell parameters, and the data collection. Raw data frames were read by SAINT (version 5/6.0)[65] and integrated using 3D profiling algorithms. A semiempirical absorption correction was applied using SADABS.[65,66] The data were corrected for Lorentz and polarization effects. Data preparation was carried out by using the program XPREP.[65] The structure was solved by direct methods and difference Fourier analysis with the use of SHELXTL 6.1.[67] Idealized positions for the hydrogen atoms were included as fixed contributions using a riding model with isotropic temperature factors set at 1.2 (aromatic protons and B−H) or 1.5 (methyl protons) times that of the adjacent nonhydrogen atom. A correction for secondary extinction was not applied. The linear absorption coefficient, atomic scattering factors, and anomalous dispersion corrections were calculated from values found in the International Tables of X-ray Crystallography.[68]

Experimental work on **2c**·$2CH_3CN$ was done at University of Minnesota (VGY). A purple needle ($0.45 \times 0.15 \times 0.15$ mm^3) was placed on the tip of a 0.1 mm diameter glass capillary and mounted on a Bruker AXS diffractometer equipped with a CCD area detector for a data collection at 173(2) K.[65] The data collection was carried out using Mo Kα radiation ($\lambda = 0.71073$ Å, graphite monochromator). The intensity data were corrected for absorption and decay (SADABS).[65,66] Final cell constants were calculated from 2796 strong reflections from the actual data collection after integration (SAINT).[65]The structure was solved by direct methods and difference Fourier analysis and refined using Bruker SHELXTL.[67] The space group $P2_1/c$was determined based on systematic absences and intensity statistics. All nonhydrogen atoms were refined with anisotropic displacement parameters. All hydrogen atoms were placed in ideal positions and refined as riding atoms with relative isotropic displacement parameters, except the borate hydrogen was allowed to refine positionally with a constrained U_{iso} relative to the host boron atom.

(65) *SMART*, V5.054; Bruker Analytical X-ray Systems: Madison, WI, 2001.
(66) For an empirical correction for absorption anisotropy, see Blessing, R. *Acta Cryst. A* **1995**, *51*, 33–38.
(67) *SHELXTL*, V6.14; Bruker Analytical X-ray Systems: Madison, WI, 2001.
(68) *International Tables for X-ray Crystallography*; Kynoch Press: Birmingham, 1974; Vol. *4*.

3. Results

3.1. General Remarks. Arylthiolate complexes were prepared by metathesis reactions of known complexes $Tp^{R,Me}Ni-Cl$ with sodium thiolate salts in weakly polar THF solvent (Scheme 1). To prevent dissociation of the Ni−SR′ bond, the lipophilic product complexes were isolated by subsequent extraction into nonpolar toluene. Elemental analyses on isolated products were consistent with formulation as $Tp^{R,Me}Ni-SR'$ (Scheme 1), and spectroscopic data described below were uniquely consistent with pseudotetrahedral complexes in paramagnetic ($S = 1$) electron configurations. This was confirmed for **1a** and **2c** by X-ray structure determinations. Cyclic voltammetry of **2b** in CH_2Cl_2 with NBu_4PF_6 electrolyte failed to elicit any redox feature within a window of ±1.2 V vs Ag/AgCl, consistent with previous results for $Tp^{iPr,iPr}Ni-SC_6F_5$.[59]

3.2. Electronic Spectroscopy. Successful formation of the various thiolate complexes in reaction solutions was initially signified by appearance of intense coloration arising from S−Ni pπ−dπ* ligand to metal charge transfer (LMCT) transitions at visible wavelengths (Figure 1). Similar bands were observed in the spectra of $Tp^{iPr,iPr}Ni-SC_6F_5$ (430 nm),[59,69] Ni(II)-substituted rubredoxin (360, 450 nm),[26,27] Ni(II)-aspartate transcarbamoylase (360, 440 nm),[30] and $[Ni(SPh)_4]^{2-}$ in CH_3CN solution (460, 510 nm).[27,28] Given the weak ligand field and electron-rich thiolates utilized in the present work, the LMCT transitions are correspondingly red-shifted. Thus, complexes supported by $Tp^{Me,Me}$ (**1a,b**) are bright red, while those of $Tp^{Ph,Me}$ (**2a**−**c**) are dark purple or blue.

In contrast to the single LMCT transition reported for $Tp^{iPr,iPr}Ni-SC_6F_5$ and related synthetic complexes,[58–60] two strong absorption bands with separations of 1000–2000 cm^{-1} were observed: **1a**, $\lambda_{max} = 464$ and 506 nm; **1b**, 467(sh) and 514 nm; **2a**, 489(sh) and 537 nm; and **2b**, 551 and 574 nm. These bands retained essentially equivalent positions and intensities in toluene, CH_2Cl_2, and CH_3CN solutions for all four complexes. The two bands of **1a**, **2b**, and **2c** had approximately equivalent extinctions, but those of **1b** and **2a** exhibited disparate values. A separate LMCT transition based on the second half-filled nickel orbital and a Ni−S pσ−d$_z^2$ bonding interaction was not suggested by DFT electronic structure calculations on $Tp^{iPr,iPr}Ni-SC_6F_5$,[69] so these observations may indicate unexpected complexity in the underlying photophysics. Nickel-thiolate stretching modes exhibit much lower energies,[69] so resolved vibrational structure within a single transition is not expected. Ligand field absorptions of $Tp^{R,Me}Ni-Cl$ (R = Me, Ph), include a strong band at 482 nm,[70] and the thiolate complexes should have an analogous band under the charge transfer features; such a band is indeed evident ($\lambda_{max} = 498$ nm, $\varepsilon = 875$ M^{-1} cm^{-1}) as a shoulder on the relatively blue-shifted CT band of $Tp^{iPr,iPr}Ni-SC_6F_5$.[69] Given the low symmetry of the

(69) Gorelsky, S. I.; Basumallick, L.; Vura-Weis, J.; Sarangi, R.; Hodgson, K. O.; Hedman, B.; Fujisawa, K.; Solomon, E. I. *Inorg. Chem.* **2005**, *44*, 4947–4960.
(70) Desrochers, P. J.; Telser, J.; Zvyagin, S. A.; Ozarowski, A.; Krzystek, J.; Vicic, D. A. *Inorg. Chem.* **2006**, *45*, 8930–8941.

Table 1. Curie Law Fits to Paramagnetic Contact Shifts for Arylthiolate Complexes

	resonance			
complex	H-4	ortho	meta	para
1a	$R^2 = 0.995$	$R^2 = 0.996$	$R^2 = 0.994$	$R^2 = 0.996$
intercept	$\delta = 7(3)$	$\delta = 3.7(8)$	$\delta = 10.0(6)$	$\delta = 2(1)$
slope	$+20.8(8) \times 10^3/T$	$-6.7(2) \times 10^3/T$	$+4.0(2) \times 10^3/T$	$-8.4(3) \times 10^3/T$
1b	$R^2 = 0.994$	$R^2 = 0.996$	$R^2 = 0.994$	$R^2 = 0.995$
	$\delta = 16(3)$	$\delta = -4(2)$	$\delta = 12.7(6)$	$\delta = 5(1)$
	$+17.5(8) \times 10^3/T$	$+11.0(4) \times 10^3/T$	$+3.8(2) \times 10^3/T$	$+6.4(3) \times 10^3/T$
2a	$R^2 = 0.999$	$R^2 = 0.998$	$R^2 = 0.999$	$R^2 = 0.999$
	$\delta = 9(1)$	$\delta = -4.9(7)$	$\delta = 10.4(3)$	$\delta = -1.8(6)$
	$+18.3(4) \times 10^3/T$	$-6.8(2) \times 10^3/T$	$+4.5(1) \times 10^3/T$	$-10.6(2) \times 10^3/T$
2b	$R^2 = 0.997$	$R^2 = 0.998$	$R^2 = 0.998$	$R^2 = 0.998$
	$\delta = 10(2)$	$\delta = -17(3)$	$\delta = 10.3(7)$	$\delta = 2(2)$
	$+17.2(5) \times 10^3/T$	$+32.5(9) \times 10^3/T$	$+6.5(2) \times 10^3/T$	$+16.4(4) \times 10^3/T$

thiolate complexes, configuration interaction between ligand field and charge transfer states may be possible, giving rise to the strong split absorptions.

Additional ligand field bands were evident at longer wavelength from the edge of the CT band: **1a**, $\lambda_{max} = 614$ and 836 nm; **1b**, $\lambda_{max} = 636$ and 861 nm; and **2a**, $\lambda_{max} = 700$ and 905 nm. Broad NIR absorptions were also found for **1a,b** at 1580 nm. Thus, the ligand field bands approximately coincide with those reported for pseudotetrahedral $Tp^{R,Me}Ni-Cl$ complexes of approximate C_{3v} geometry.[63,70] Additional bands of intermediate extinction in the near UV are absent in the chloride complex precursors, and thus can be plausibly assigned to intraligand transitions within the aromatic thiolate substituents.

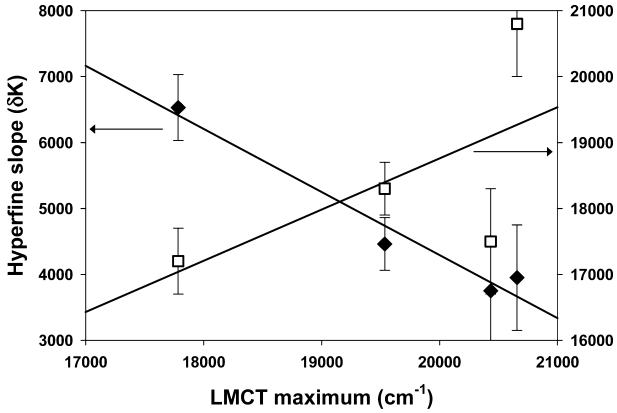

Figure 3. Plot of averaged LMCT band energies of **1a,b** and **2a,b** versus hyperfine slopes for arylthiolate meta resonances (♦, left axis) and 4-pyrazolyl resonances (□, right axis).

Table 2. Summary of the Crystal Data and Structure Refinements

complex	$Tp^{Me,Me}Ni-SPh$ (**1a**)	$Tp^{Ph,Me}Ni-SXyl$ (**2c**)·$2CH_3CN$
empirical formula	$C_{21}H_{27}BN_6NiS$	$C_{42}H_{43}BN_8NiS$
formula weight	465.07	762.42
crystal size, mm	$0.10 \times 0.21 \times 0.58$	$0.45 \times 0.15 \times 0.15$
T, K	293(2)	173(2)
crystal system	orthorhombic	monoclinic
space group	*Pbca*	$P2_1/c$
a, Å	15.259(2)	10.8543(3)
b, Å	14.427(1)	39.977(3)
c, Å	21.182(2)	10.1747(8)
α, deg	90	90
β, deg	90	114.972(1)
γ, deg	90	90
V, Å^3	4662.9(8)	4002.3(5)
Z	8	4
D_{calc}, g cm^{-3}	1.325	1.264
2θ range, deg	2.17−27.49	2.04–27.51
μ (Mo Kα), mm^{-1}	0.941	0.577
R1, wR2 ($I > 2\sigma(I)$)	0.0401, 0.1061	0.0402, 0.0949
R1, wR2 (all data)	0.0614, 0.1246	0.0579, 0.1008

A red-shift of the LMCT and ligand field bands can be noted in order of increasing steric bulk of the $Tp^{R,Me}Ni-SR'$ complexes. For example, the LMCT features lie at notably lower energies for R = Ph compared to R = Me, as also observed in trigonal-bipyramidal complexes,[61] and secondarily for R′ = Mes compared to Ph as well. This trend might reflect weaker pyrazolyl σ-donor strength afforded to nickel(II) due to an opened ligand bite accommodating the larger 3-pyrazolyl substituent for R′ = Ph, as well as enhanced thiolate basicity for R = Mes. However, the presence of ortho-thiolate substituents alone induces the LMCT shift evident between spectra of **2a** and **2b,c**. We conclude that contact between the 3-pyrazolyl and ortho-thiolate substituents perturbs Ni−S bonding, resulting in a significant contribution to observed LMCT red shifts.

3.3. ^{1}H NMR Spectroscopy. Complexes **1a,b**, **2a−c**, and their precursor chloride complexes all exhibited well-resolved ^{1}H NMR spectra at room temperature in $CDCl_3$ solutions, notwithstanding their paramagnetic electronic configurations (Figure 2). $Tp^{Me,Me}NiCl$ exhibited four expected signals: a relatively sharp resonance at 6.0 ppm assigned to the 5-methyl protons; a much broader resonance at −8.1 ppm assigned to the 3-methyl protons proximal to the metal ion; a borohydride resonance at −12.9 ppm; and a 4-pyrozolyl ring proton resonance shifted significantly downfield to 81.9 ppm. Compared to the chloride complex, the spectrum of **1a** in $CDCl_3$ contains three additional signals at 23.7, −18.9, and −26.6 ppm respectively assigned to the meta, ortho, and para protons of the phenylthiolate ligand on the basis of their relative intensities and linewidths in relation to expected spatial separation from the $S = 1$ nickel(II) ion. The alternating upfield, downfield, upfield pattern in the arylthiolate proton shifts reflects a predominant contact shift mediated by spin polarization,[46,55,60,71,72] consistent with residence of the unpaired electrons in a nondegenerate configuration exhibiting S−Ni $p\pi-d\pi^*$ overlap.[69] Introduction of ortho and para methyl substituents on the mesitylthiolate ligand of **1b** causes expected reversal of the spin polarity at these positions, resulting in three downfield signals

(71) Jesson, J. P. *J. Chem. Phys.* **1967**, *47*, 582–591.
(72) Horrocks, W. D., Jr.; Greenberg, E. S. *Inorg. Chem.* **1971**, *10*, 2190–2194.

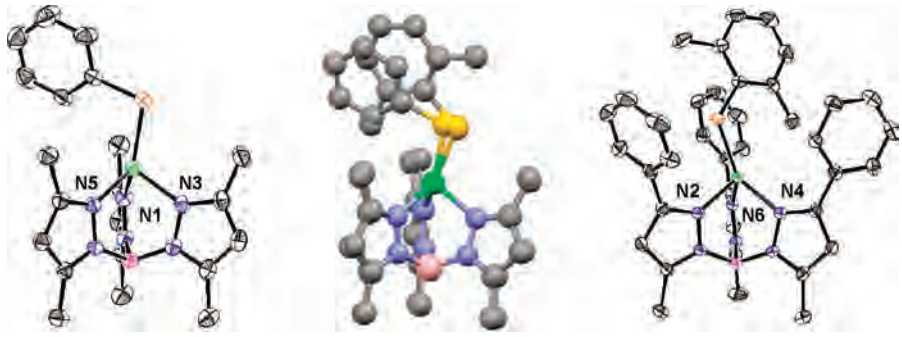

Figure 4. ORTEP plots for $Tp^{Me,Me}Ni-SPh$ (**1a**, left) and $Tp^{Ph,Me}Ni-SXyl$ (**2c**, right) with thermal ellipsoids drawn at 30% probability. A least-squares superposition of the structures is shown at center to highlight differential thiolate coordination; for clarity, only the ipso carbons of the 3-Ph substituents are shown for **2c**.

Table 3. Summary of Significant Bond Lengths and Angles

Complex			
$Tp^{Me,Me}Ni-SPh$ (**1a**)		$Tp^{Ph,Me}Ni-SXyl$ (**2c**)	
Bond Lengths			
Ni1−S1	2.216(1)	Ni1−S1	2.1978(5)
Ni1−N3	1.992(2)	Ni1−N2	2.032(2)
Ni1−N1	1.978(2)	Ni1−N4	2.019(2)
Ni1−N5	1.988(2)	Ni1−N6	2.030(2)
S1−C16	1.771(2)	S1−C31	1.775(2)
Bond Angles			
S1−Ni1−N3	113.26(6)	S1−Ni1−N2	103.05(5)
S1−Ni1−N1	134.69(6)	S1−Ni1−N4	135.73(5)
S1−Ni1−N5	122.69(6)	S1−Ni1−N6	129.95(5)
N1−Ni1−N3	90.25(8)	N2−Ni1−N4	89.70(6)
N3−Ni1−N5	92.49(8)	N2−Ni1−N6	91.02(6)
N1−Ni1−N5	92.48(8)	N4−Ni1−N6	91.23(6)
Ni1−S1−C16	103.84(8)	Ni1−S1−C31	116.51(7)

at 33.27 (ortho), 25.8 (para), and 25.3 (meta). Analogous results were also obtained for the series of $Tp^{Ph,Me}$ complexes. Thus, the precursor chloride complex exhibited six resonances: signals at 78.6, 4.4, and −13.7 ppm correspond to the 4-pyrazolyl, 5-methyl, and borohydride protons; three more at 9.7, 8.7, and 8.0 ppm correspond to the ortho, meta, and para protons of the 3-phenyl substituents. The latter three signals increasingly broaden with increasing proximity to the metal center, with the ortho resonance being particularly broad. The complexes **2a**−**c** exhibit three additional resonances due to the arylthiolate protons, with contact shifts again determined by spin polarization.

In comparing the various ^1H NMR spectra, shifts of the tris(pyrazolyl) ligand resonances are smaller in magnitude for $Tp^{Ph,Me}$ complexes compared to $Tp^{Me,Me}$ analogs, and also for thiolate complexes compared to their chloride complex precursors. For example, the chemical shifts of the 4-pyrazolyl protons of $Tp^{Me,Me}Ni-Cl$, **1a** and **1b**, are 81.9, 77.2, and 75.0 ppm, respectively (Figure 2), compared to 78.6, 70.8, and 67.0 ppm for their $Tp^{Ph,Me}$ analogs. Conversely, the arylthiolate protons show an opposing trend; the common arylthiolate meta protons resonate at 23.3, 25.3, 25.5, 32.2, and 32.9 ppm for **1a**, **1b**, **2a**, **2b**, and **2c**, respectively. The latter effect is particularly dramatic for **2b,c** which incorporate both the bulkier $Tp^{Ph,Me}$ ligand and an ortho-disubstituted arylthiolate: the ortho-methyl protons of **2b** and **2c** resonate at 92 and 97 ppm respectively, compared to 33 ppm for **1b**. These trends may arise from competing factors. Steric contact between the thiolate and the pyrazolyl substituents may reduce covalency of the Ni−N coordinate bonds, attenuating spin density on the pyrazolyl rings. Such steric contacts may alternatively perturb thiolate coordination, causing the arylthiolate ligands to accept more spin density through enhanced covalency in the S−Ni $p\pi-d\pi^*$ bond, reducing shifts of the tris(pyrazolyl)borate ligand protons relative to a chloride complex.

In order to clearly delineate these trends, chemical shifts were determined as a function of temperature over a 265–300 K range for the 4-pyrazolyl protons on the Tp ligands, and the ortho, meta, and para positions of the arylthiolates for complexes **1a,b** and **2a,b**. The data were fit by least-squares techniques to linear functions according to the Curie law, and the results are summarized in Table 1. Obtained slopes (i.e., hyperfine constants) correlate with the averaged S−Ni $p\pi-d\pi^*$ LMCT energies for each complex (Figure 3). The absence of significant shift effects from zero-field splitting was evident from linearity of the Curie plots, and the observed trends also suggest predominance of through-bond contact shifts over dipolar shifts, both consistent with spin Hamiltonian parameters reported for $Tp^{Me,Me}Ni-Cl$.[70] An inverse dependence was evident in the common meta resonance on the arylthiolate ligands (i.e., **1a** < **1b** < **2a** < **2b**), thus implying a significant steric effect on Ni−SR′ covalency, consistent with an opposing trend for the 4-pyrazolyl protons (i.e., **1a** ≥ **2a** ≥ **2b**). These results are consistent with significant steric perturbation of the nickel-thiolate coordinate bond.

3.4. X-ray Crystallography. To further elucidate this steric effect, structures were determined by X-ray crystallography for complexes **1a** and **2c** (Figure 4 and Table 3). Both complexes adopt severely distorted pseudotetrahedral geometries in which the Ni−S bonds are significantly bent from an ideal trigonal axis toward one pyrazole ring, as previously reported for $Tp^{iPr,iPr}Ni-SC_6F_5$.[59] The aromatic thiolate substituents are disposed backward over the edge between the two distal pyrazoles, and are nearly coplanar with the Ni−S bonds (torsion angles ±15.2° for **1a**; ±16.4° for **2c**), yielding approximate C_s symmetry. The Ni−S bond length of **1a** is slightly longer than that of **2c**, 2.216(1) and 2.1978(5) Å, respectively. Conversely, the Ni−N bonds of **1a** are very slightly shorter than those of **2c**, averaging 1.986(7) and 2.027(7) Å, respectively, compared to 1.98(2) and 1.99(1) Å in the chloride complex precursors

$Tp^{R,Me}Ni-Cl$, (R = Me, Ph respectively).[62,63] Moreover, the N−Ni−N angles remain close to 90° for both complexes (averaging 90.7(8)° for **2c** and 92(1)° for **1a**), owing to the constrained bite imposed upon the Tp ligand by the borate tether. Given displacement of the thiolate donors off the trigonal axis, the N−Ni−S angles vary widely (Table 3).

Reflecting the increased basicity of the arylthiolates utilized in the present work compared to the perfluoroaryl analog, the Ni−S bond lengths of **1a** and **2c** are significantly shorter than that of $Tp^{iPr,iPr}Ni-SC_6F_5$ (2.259(2) Å),[59] and also those of $[Ni(SAr)_4]^{2-}$ (2.26–2.33 Å),[54–57] consistent with reduced complex charge. Ni−S bond lengths of 2.236(1) and 2.187(1) Å were recently reported for $PhB(CH_2S^tBu)_3$-Ni−SAr (Ar = C_6F_5 and C_6H_5, respectively).[60] A shorter Ni−S bond length of 2.119(1) Å was found in the pseudotetrahedral complex $PhB(CH_2PPh_2)_3Ni-SC_6H_4$-*p*-^{t}Bu; aside from the distinctive donor set of this complex, the Ni−S coordinate bond is bent over an edge between donor atoms and the arylthiolate substituent adopts a perpendicular orientation (torsion angles: 113°, −69°).

As anticipated from spectroscopic results, there are clear and instructive differences between the sterically unhindered arylthiolate ligation of **1a** and that of the more encumbered **2c** (Figure 4, center). Most obviously, the bond angle at sulfur (i.e., Ni−S−C) is significantly increased, from 103.84(8)° in **1a** to 116.51(7)° in **2c**, and tilting of the thiolate bond off the trigonal axis toward a proximal pyrazole nitrogen becomes even more pronounced (N3−Ni1−S1 = 113.26(6)° in **1a**, N2−Ni1−S1 = 103.05(5)° in **2c**). The Cambridge Database presently returns exactly 100 values for bond angles about sulfur for terminal arylthiolate ligands on nickel; these range from 99.146° to 121.038°, of which only 9 are smaller than that of **1a** and only three exceed that of **2c**. Hence, **1a** and **2c** together nearly span the known coordination space available to arylthiolates at a single nickel center. The steric hindrance in **2c** arises from short contacts between the thiolate and the 3-phenyl substituents on the supporting ligand, which are rotationally disposed to form a three-sided box about the xylyl substituent. The sulfur atom itself is wedged against the central 3-phenyl ring, resulting in a distance of only 3.29 Å to the ipso carbon. This distance plausibly represents the sum of van der Waals radii. Distances between the inner ortho-xylyl carbon on the thiolate and the two flanking 3-Ph rings include carbon−carbon contacts as short as 3.45 Å.

The nickel ion itself also provides a short contact to the ortho methyl at a distance of 3.10 Å, supporting a Ni···H−C distance of 2.56 Å that is disposed nearly axially toward the proximal pyrazole (N2−Ni1···H38A = 163.9°). Similarly short ortho-fluorine contacts (ca. 2.56–2.64 Å) within related perfluoroarylthiolate complexes were previously dismissed as nonbonding.[73] While unusual low-energy ν(C−H) IR modes indicative of agostic bonding were not observed in the present work,[74,75] weak electrostatic ("anagostic")[76] interaction with the hydrocarbyl substituents does seem plausible.[77–79] Moreover, the dissimilar dispositions of arylthiolate ligands in **1a** and **2c** place their respective ortho and xylyl methyl carbons in nearly equivalent positions relative to nickel (Figure 4 center), so a short Ni···H−C distance of 2.72 Å is also found in **1c** between the ortho proton and nickel, at an angle of 173.1° to N3 on the proximal pyrazole.

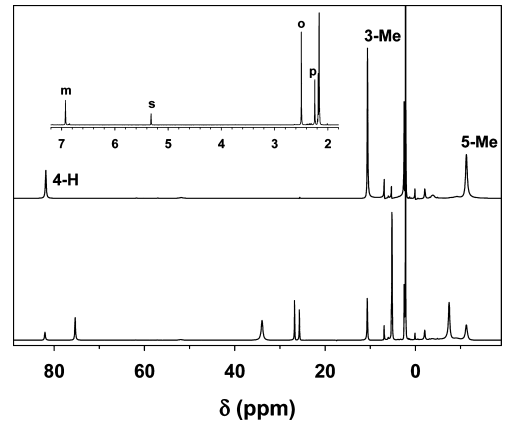

Figure 5. ^{1}H NMR spectra for reaction of $Tp^{Me,Me}Ni-SMes$ and MeI in CD_2Cl_2 at 295 K, near the start (bottom) and near equilibrium (top). The inset shows spectrum of mesitylmethylsulfide coproduct recorded using routine acquisition parameters for a diamagnetic solvate.

3.5. Electrophilic Alkylation. Reactivities of **1a** and **2b** with methyl iodide were also examined to further probe the steric manipulation of their respective nickel-thiolate bonds. Addition of excess MeI to a CD_2Cl_2 solution of **1b** at room temperature resulted in clean decomposition to form a paramagnetic halide complex and free MeSMes as observed by ^{1}H NMR spectroscopy (Figure 5). Conversion of **1a** and **2b** to respective $Tp^{R,Me}Ni-I$ (R = Me, Ph) product complexes was monitored by UV–visible spectrophotometry (Figure 6); the equilibrium spectrum of the $Tp^{Me,Me}Ni-I$ concurred with previous results,[70] while the identity of $Tp^{Ph,Me}Ni-I$ was inferred by comparison to the chloride complex.[61,70] Kinetic measurements for alkylations were made under pseudofirst-order conditions (i.e., $-d[Tp^{R,Me}Ni-SR']/dt = k_{obs}[Tp^{R,Me}Ni-SR']$, where $k_{obs} = k_1 + k_2[MeI]_0$; $[Tp^{R,Me}Ni-SR']_0$ = 0.5 mM, $[MeI]_0$ = 16–128 mM), and linear dependences for observed rate as a function of methyl iodide concentrations were obtained by global least-squares fittings to single exponentials for both complexes (Figure 7). The second-order rate constant obtained for the sterically hindered complex **2b** was 10-fold larger, $k_2 = 1.23(8) \times 10^{-3}$ M^{-1} s^{-1} vs $1.20(3) \times 10^{-4}$ M^{-1} s^{-1} for **1a**. A significant zero-order intercept was extrapolated for

(73) Thompson, J. S.; Sorrell, T.; Marks, T. J.; Ibers, J. A. *J. Am. Chem. Soc.* **1979**, *101*, 4193–4200.
(74) Trofimenko, S.; Calabrese, J. C.; Thompson, J. S. *Inorg. Chem.* **1992**, *31*, 974–979.
(75) Alvarez, H. M.; Krawiec, M.; Donovan-Merkert, B. T.; Fouzi, M.; Rabinovich, D. *Inorg. Chem.* **2001**, *40*, 5736–5737.
(76) Brookhart, M.; Green, M. L. H.; Parkin, G. *Proc. Natl Acad. Sci. USA* **2007**, *104*, 6908–6914.
(77) Soong, S.-L.; Hain, J. H., Jr.; Millar, M.; Koch, S. A. *Organometallics* **1988**, *7*, 556–557.
(78) Youngs, W. J.; Kinder, J. D.; Bradshaw, J. D.; Tessier, C. A. *Organometallics* **1993**, *12*, 2406–2407.
(79) Shan, X.-F.; Wu, L.-Z.; Liu, X.-Y.; Zhang, L.-P.; Tung, C.-H. *Eur. J. Inorg. Chem.* **2007**, 3315–3319.

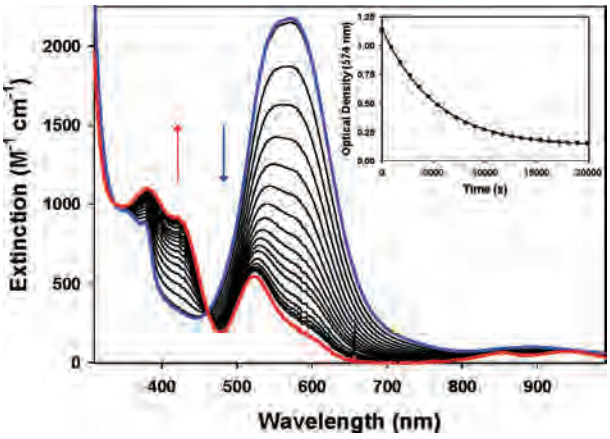

Figure 6. UV–visible traces for reaction of $Tp^{Ph,Me}Ni-SMes$ (**2b**, 0.5 mM) with MeI (128 mM) at 295 K in CH_2Cl_2 solution (Δt = 900 s). Limiting traces shown in blue and red are calculated spectra of the starting thiolate and product $Tp^{Ph,Me}Ni-I$ complexes, respectively. The inset shows a single-exponential fit by global least-squares techniques to the time-dependent optical density at 574 nm (λ_{max} for **2b**).

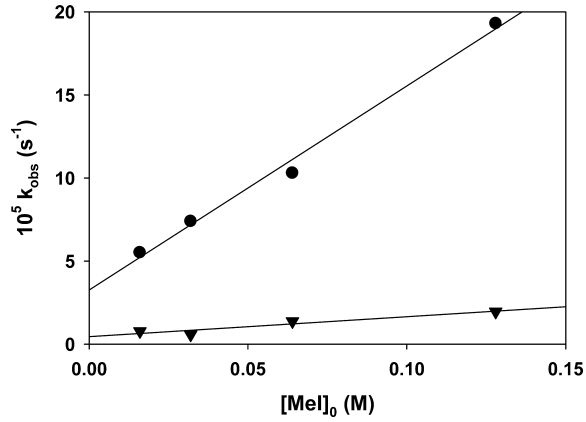

Figure 7. Dependence of methyl iodide concentration on rate of decomposition ($k_{obs} = k_1 + k_2[MeI]$) for $Tp^{Me,Me}Ni-SPh$ (**1a**, ▼, R^2 = 0.91) and $Tp^{Ph,Me}Ni-SPh$ (**2b**, •, R^2 = 0.99) in CH_2Cl_2 solution at 297 K.

2b, $k_1 = 3.3(6) \times 10^{-5}$ s^{-1}, while that for **1a** was again smaller, $5(2) \times 10^{-6}$ s^{-1}.

These results are interpreted to represent an unprecedented superposition of competing mechanisms (Scheme 2): bimolecular nucleophilic reaction between intact complex and methyl iodide that gives rise to the first-order (i.e., linear) rate dependence on the latter, and a rate-limiting dissociation of the nickel−thiolate bond that is followed by rapid (i.e., saturated and effectively zero-order) alkylation of the displaced thiolate that gives rise to the intercept.[48] The enhanced basicity of mesityl thiolate is likely to contribute to the larger k_2 bimolecular rate constant observed for **2b** in comparison to **1a**, but also would be expected provide an opposing effect on the k_1 unimolecular path. These results thus demonstrate a significant steric effect on reaction kinetics, consistent with perturbation of Ni(II)−SAr coordinate bonding already evident in the spectroscopic and structural data.

4. Discussion

The prominent feature of the thiolate complex structures is the tilting of the Ni−S bond vector off the trigonal axis,

Scheme 2

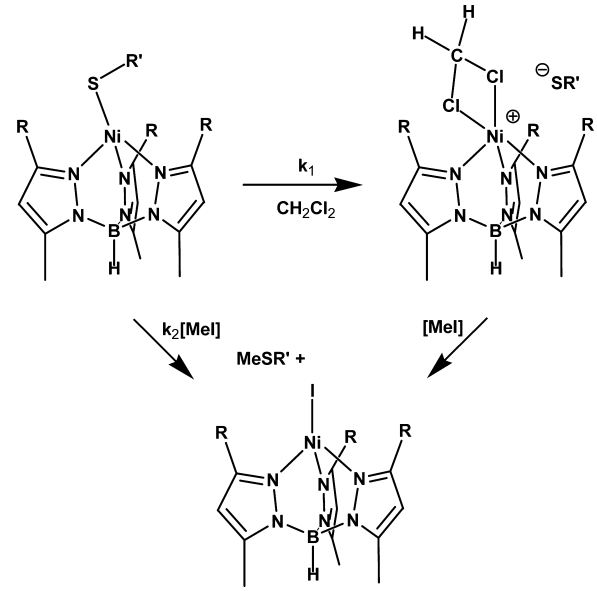

which is accentuated by steric effects in the bulkier complex **2c**. In light of the attendant spectroscopic trends already elucidated, the effects of this geometric distortion on the electronic structure of the complexes can be considered in a qualitative sense based on symmetry considerations. Cogent density functional theory (DFT) analyses have already been reported for spectroscopy and bonding of Ni(II) arylthiolate complexes in tetrahedral and square pyramidal geometries,[48,69] which serve as a starting point for such deliberation. The pseudotetrahedral chloride complex precursors exhibit nearly perfect 3-fold symmetry,[62,63] but the arylthiolate substituents break axial symmetry, enabling the observed reduction in symmetry from C_{3v} to C_s. The thiolate ligands accordingly present two unhybridized sulfur p orbitals toward the metal ion of σ and π symmetry; the sulfur pσ orbital is destabilized by interaction with a lower-lying, filled nickel dσ orbital, the other p orbital effects net covalent pπ−dπ* bonding with a half-filled d orbital, and the second half-filled d orbital is essentially nonbonding.[69] Of course, the σ and π symmetries and bonding interactions are exactly reversed in a square pyramid.[48] Tilting of the Ni−S bond vector off the trigonal axis toward one vertex will reduce the destabilizing axial pσ−dσ* overlap in a pseudotetrahedron, but the cylindrical symmetry of the single pπ−dπ* bonding interaction would be unaffected. Therefore, covalency of the Ni−SR′ coordinate bond should increase with the degree of tilting and indeed, a slightly shortened bond distance is observed in **2c** compared to **1a**. The orbital effects of an opposing tilt, away from a trigonal vertex toward an edge between nitrogen donors, were explicitly modeled for isoelectronic TpCo(CO) using Extended Hückel theory;[80] such a structure has been observed experimentally in $PhB(CH_2PPh_2)_3Ni-SC_6H_4$-*p*-^{t}Bu.[58] Steric effects can profoundly perturb the geometric and electronic structures; for

(80) Detrich, J. L.; Konečný, R.; Vetter, W. M.; Doren, D.; Rheingold, A. L.; Theopold, K. H. *J. Am. Chem. Soc.* **1996**, *118*, 1703–1712.
(81) Jenkins, D. M.; Peters, J. C. *J. Am. Chem. Soc.* **2005**, *127*, 7148–7165.

example, axial Jahn–Teller distortion can be preferentially enforced over trigonal bending by the presence of very bulky arylthiolate substituents in the low spin ($S = ½$) state of related cobalt(II) complexes.[81]

Electrophilic alkylation of thiolate complexes are of interest in regard to analogous biological alkyl transfers to zinc thiolate centers such as that in the Ada DNA repair protein.[82–85] Comparative reactivities of zinc and nickel model complexes have been studied to determine kinetic and mechanistic effects arising from covalency of the Ni−S bond.[46,48] Two limiting reaction mechanisms for electrophilic thiolate alkylation have been identified: rate-limiting dissociation of a thiolate ligand from the metal center (i.e., k_1 in Scheme 2), typified by the dianionic complexes $[Zn(SR)_4]^{2-}$ [84] and direct bimolecular reactions (i.e., k_2 in Scheme 2) of intact neutral complexes (κ^3-L)Zn-SR,[85] as well as of cationic complexes $[(\kappa^4\text{-L})\text{M-SR}]^+$ (M = Ni, Zn).[48] The dianionic charge of the former assists a unique thiolate dissociation pathway,[84] and the effects of solvent polarity also should be considered.[46]

We were nonetheless surprised to find unprecedented evidence in the present work that both mechanisms are competitive in reactivity of the neutral pseudotetrahedral nickel(II) complexes (Scheme 2). Both pathways are accelerated by an order of magnitude due to the steric congestion introduced in complex **2b** in comparison to **1a**, notwithstanding the shorter Ni−S bond length in the former. In contrast, square-pyramidal RSRS-$[(\kappa^4\text{-tmc})\text{Ni}-\text{SPh})]^+$ (tmc = 1,4,8,11-tetra-*N*-methyl-tetraazacyclotetradecane) with a shorter Ni−SPh bond reacts 300-fold more slowly with C_2H_5I than the RRSS isomer.[46] Significant effects within pseudotetrahedral complexes arising from varied thiolate substituents and tripodal supporting ligands were previously reported for bimolecular reaction rates of neutral zinc complexes;[85] the observed rate of reaction for MeI with $Tp^{Ph,Me}Zn-SPh$ (the analog of **2a**) was 2.0×10^{-3} M^{-1} s^{-1} (in $CHCl_3$ at 300 K), approximating the value of k_2 observed for **2b**. Curiously, the bulkier $Tp^{tBu,Me}Zn-SPh$ complex reacted 200 times more slowly than $Tp^{Ph,Me}Zn-SPh$, reflecting steric protection of the Zn−S bond from MeI within a hydrophobic pocket; unfortunately, we were unable to obtain stable nickel analogs incorporating this supporting ligand by chloride metathesis. Similar rates of reaction were also observed for reaction of benzyl bromide in CH_3CN with a pair of square-pyramidal complex analogs (κ^4-L)M-SAr [M = Ni, Zn, L = 1,5-bis(2-pyridylmethyl)-1,5-diazacyclooctane].[48]

The disparate effects of complex charge, geometry, bonding and sterics on the Ni−SR′ bond stabilities underscore the rich mechanistic behavior of the superficially straightforward alkylation reactivity. Full elucidation of the factors controlling this chemistry remains to be completed. Nevertheless, the surprising dissociative reactivity of thiolate from the uncharged nickel complexes in low-polarity solvent observed in the present work recalls the lability of the proximal site in the ACS A-cluster[6–8,13–16] and may also reflect the lack of pseudotetrahedral nickel enzyme sites akin to zinc fingers.[31]

5. Conclusions

Five pseudotetrahedral nickel(II) arylthiolate complexes $Tp^{R,Me}Ni-SR'$ (R = Me, Ph; R′ = Ph, 2,4,6-Mes, 2,6-Xyl) were prepared and fully characterized. Manipulation of steric bulk at the opposing 3-pyrazoyl and ortho-arylthiolate positions within this series gives rise to a range of electronic structures as revealed by UV–visible-NIR and paramagnetic ^{1}H NMR spectra, as well as by X-ray crystallography of two examples at steric extremes of this series. Increasing steric bulk gives rise to structural distortion of the nickel(II)-thiolate bond consisting of a significantly increased tilting of the Ni−S bond from trigonal symmetry and increased linearity of the Ni−S−R angle. This distortion alters covalency of the Ni−S coordinate bond, as revealed by red-shifted LMCT bands and enhanced hyperfine contacts onto the arylthiolate substituent. Reactivity of the nickel-thiolate linkage toward electrophilic alkylation is also significantly enhanced along two distinct pathways, a direct reaction of intact complex and rate-limiting thiolate dissociation.

Acknowledgment. This work was supported by a startup grant from Ohio University (M.P.J.).

Supporting Information Available: Crystallographic data for $Tp^{Me,Me}Ni-SC_6H_5$ (**1a**) and $Tp^{Ph,Me}NiS\text{-}2,6\text{-}C_6H_3(CH_3)_2\cdot 2CH_3CN$ (**2c**·$2CH_3CN$) in CIF format. This material is available free of charge via the Internet at http://pubs.acs.org.

IC702417W

(82) Parkin, G. *Chem. Rev.* **2004**, *104*, 699–767.
(83) Wilker, J. J.; Lippard, S. J. *J. Am. Chem. Soc.* **1995**, *117*, 8682–8683.
(84) Wilker, J. J.; Lippard, S. J. *Inorg. Chem.* **1997**, *36*, 969–978.
(85) Rombach, M.; Seebacher, J.; Ji, M.; Zhang, G.; He, G.; Ibrahim, M. M.; Benkmil, B.; Vahrenkamp, H. *Inorg. Chem.* **2006**, *45*, 4571–4575.